

Electrical spin injection and transport in germanium

Yi Zhou,^{1,*} Wei Han,^{2,*} Li-Te Chang,¹ Faxian Xiu,¹ Minsheng Wang,¹ Michael Oehme,³ Inga A. Fischer,³ Joerg Schulze,³ Roland. K. Kawakami,² and Kang L. Wang^{1,†}

¹*Device Research Laboratory, Department of Electrical Engineering, University of California, Los Angeles, California 90095, USA*

²*Department of Physics and Astronomy, University of California, Riverside, California 92521, USA*

³*Institut fuer Halbleitertechnik (IHT), Universitaet Stuttgart, Stuttgart, 70569, Germany*

(Received 7 September 2011; published 30 September 2011)

We report the first experimental demonstration of electrical spin injection, transport, and detection in bulk germanium (Ge). The nonlocal magnetoresistance (MR) in n-type Ge is observable up to 225 K. Our results indicate that the spin relaxation rate in the n-type Ge is closely related to the momentum scattering rate, which is consistent with the predicted Elliot-Yafet spin relaxation mechanism for Ge. The bias dependence of the nonlocal MR and the spin lifetime in n-type Ge is also investigated.

DOI: [10.1103/PhysRevB.84.125323](https://doi.org/10.1103/PhysRevB.84.125323)

PACS number(s): 85.75.-d, 72.25.Dc, 72.25.Hg, 81.05.Cy

I. INTRODUCTION

Information processing based on the electron's spin degree of freedom is envisioned to offer a new paradigm of electronics beyond the conventional charge-based device technologies.^{1,2} Adding spin functionality into semiconductor-based field effect transistors (e.g., spin-FET)³⁻⁵ is considered as one of the approaches to overcome the ultimate scaling limits of the mainstream silicon (Si)-based complementary metal-oxide-semiconductor (CMOS) technology.⁶ Electrical injection and transport of spin-polarized electrons from ferromagnetic metals (FMs) into the semiconductors is a prerequisite for developing such an approach.^{1,2} Recently, significant progress has been made in Si,⁷⁻¹⁰ showing great promise for achieving spintronic devices beyond the CMOS technology. On the other hand spintronics based on SiGe heterostructures would likely offer more opportunities by taking advantage of the higher carrier mobility, device design flexibility, and tunable spin relaxation¹¹ rendered by the strain engineering and bandgap engineering, as well as the quantum confinement effects while maintaining the CMOS compatibility. However, despite the success of Si spintronics, the feasibility of SiGe spintronics remains an open question because Ge is expected to have faster spin relaxation than that of Si due to the larger spin-orbit interaction. Furthermore, electrical spin injection and transport in either Ge or SiGe heterostructures have not yet been clearly demonstrated.

In this paper we report the first demonstration of electrical spin injection to bulk Ge by using an epitaxially grown Fe/MgO/n-Ge tunnel junction. The observation of Hanle spin precession in the nonlocal geometry provides unambiguous evidence of spin injection and transport in Ge. The nonlocal magnetoresistance (MR) in Ge is observed up to 225 K. Both the nonlocal MR and the spin lifetime are found to be weakly dependent on temperature at low temperature region ($T < 30$ K). However, the dependence becomes much stronger as the temperature increases. This is attributed to the dominance of spin relaxation by ionized impurity scattering at low temperatures and phonon scattering at higher temperatures. Our results show a close relation between the spin relaxation rate and the momentum relaxation rate, which is consistent with the predicted Elliot-Yafet spin relaxation mechanism for Ge.^{12,13} We also examine the bias dependence of the nonlocal

MR and spin lifetime. The smaller nonlocal MR under forward biases are attributed to the fast spin relaxation rate in the highly doped Ge-surface layer and a possible lower spin injection efficiency due to the unscreened electric field in the semiconductor. Our results show that Ge is also a promising candidate for spintronics and thus opens up the possibility of using SiGe for spintronic applications.

II. EXPERIMENTAL DETAILS

An unintentionally doped n-type Ge wafer is used as the starting substrate. A lightly doped n^- ($n = 1 \times 10^{16} \text{cm}^{-3}$) Ge layer (300 nm) is grown on this substrate as the spin transport channel. Above this layer is a transition layer (15 nm) to a degenerately doped n^+ ($n = 2 \times 10^{19} \text{cm}^{-3}$) surface layer (15 nm). All these layers are grown by low-temperature solid-source molecular beam epitaxy.¹⁴ Two devices (A and B) are fabricated on this wafer with the same processes. First a device channel is defined by photolithography and etched by reactive ion etching. The width of the channel is 5 μm and 15 μm for devices A and B, respectively. The height of the channel mesa is 60 nm for both devices. Four electrodes are then fabricated on the channel by the standard e-beam lithography and liftoff process. The outer two electrodes are made of Au/Ti. The center two spin-dependent electrodes are made of MgO (1 nm) and Fe (100 nm), which are deposited in a molecular beam epitaxy system and capped by 5 nm Al_2O_3 . The as-grown MgO is single crystalline and possesses a 45 degree in-plane rotation of the unit cell with respect to that of the Ge.¹⁵ A schematic of the atomic configuration is shown in Fig. 1(a). This high quality Fe/MgO/Ge junction not only alleviates the Fermi-level pinning at the Ge surface to favor electronic transport¹⁶ but also leads to an enhanced spin polarization of the injected electrons due to the symmetry-induced spin filtering.¹⁷ To characterize the spin injection and transport in Ge, we employ the nonlocal measurement technique.¹⁸⁻²² The center-to-center distance (L) between the spin injector (E2) and spin detector (E3) is 420 nm and 1 μm for device A and device B, respectively. A schematic diagram of the device structure and measurement scheme is shown in Fig. 1(b). The standard low-frequency lock-in technique is used for the measurement.

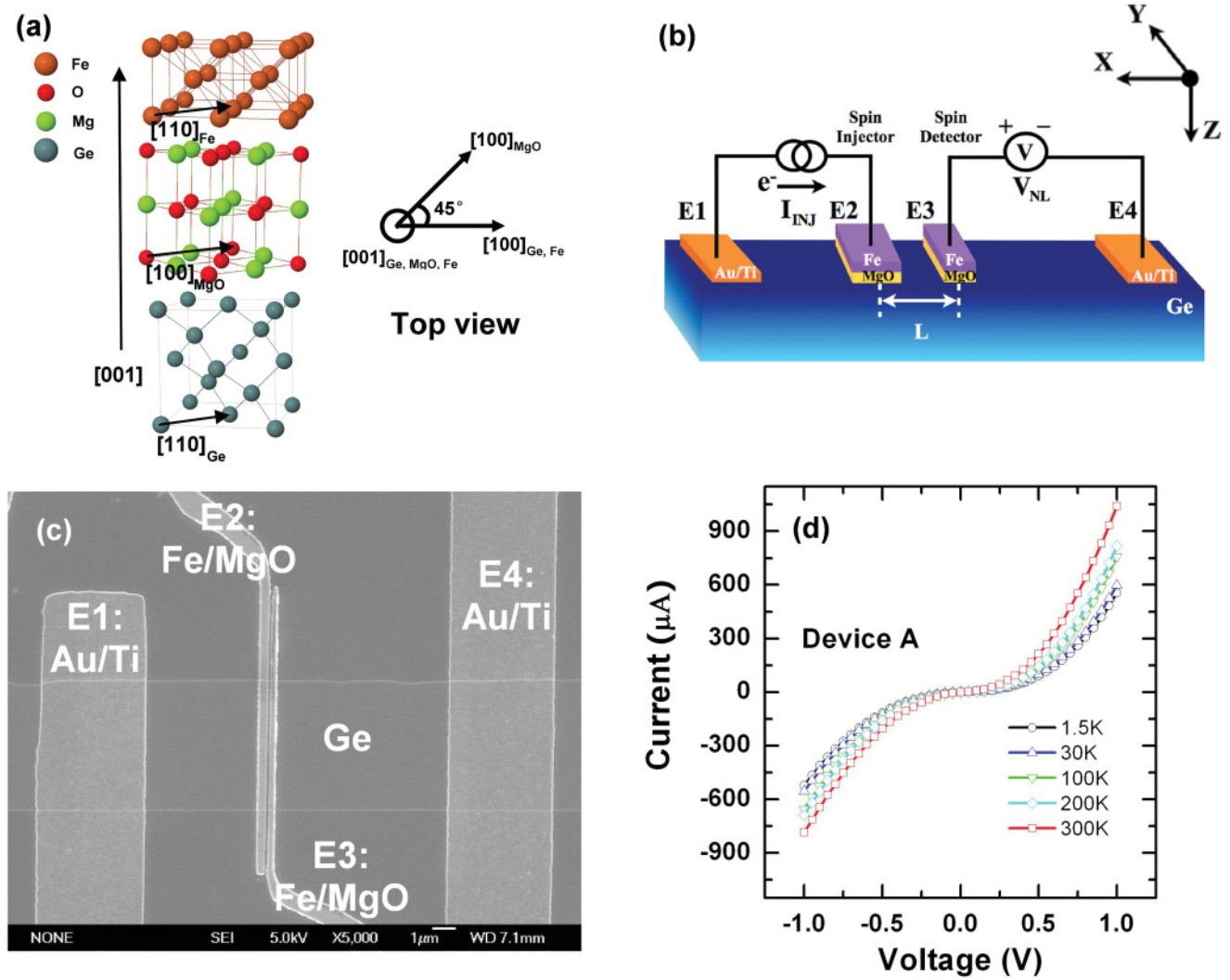


FIG. 1. (Color online) (a) Schematic atomic configuration of the Fe/MgO/Ge junction, showing 45 degree rotation of the MgO unit cell with respect to that of Ge. (b) A schematic diagram of the device structure and the nonlocal measurement scheme. The center-to-center distances between the spin injector and detector are 420 nm and 1 μ m for devices A and B, respectively. (c) A SEM image of device A. The widths of the injector (E2) and detector (E3) are 400 nm and 250 nm, respectively. (d) Temperature-dependent I - V curves measured between spin injector (E2) and E1.

III. RESULTS AND DISCUSSION

A. Electrical characterization

Figure 1(c) shows a scanning electron microscope (SEM) image of the device A. The widths of the spin injector (E2) and spin detector (E3) are 400 nm and 250 nm, respectively. Temperature-dependent I - V characteristics measured between the spin injector (E2) and E1 are shown in Fig. 1(d). Since E1 is made of Au/Ti and the size is much larger than E2, we consider that the I - V characteristics are dominated by the contact resistance of the spin injector (E2). The nonlinearity and weak-temperature dependence of the I - V characteristics confirm the tunneling nature of this contact,²³ which is necessary to overcome the conductivity mismatch problem for spin injection from FMs to semiconductors.²⁴⁻²⁶

B. Non-local spin valve measurement

To characterize spin injection and transport in Ge, we first perform the nonlocal spin valve measurement. In this measurement a charge current is applied between the spin injector (E2) and E1 [as shown in Fig. 1(b)], resulting in a spin accumulation in the Ge at E2 by means of spin injection (E2 under a reverse bias) or spin extraction (E2 under a forward bias).^{27,28} In either case once spin accumulation is created, the spin-polarized electrons start to diffuse isotropically in the Ge channel. The spin detector (E3) is placed outside the charge current path, and it detects a voltage potential that is proportional to the projection of the spin accumulation in the Ge onto its magnetization direction. Therefore, if the spin accumulation of the injected electrons is sizeable when they diffuse to E3, a bipolar nonlocal voltage V_{NL} should be observed, which changes sign when the magnetization

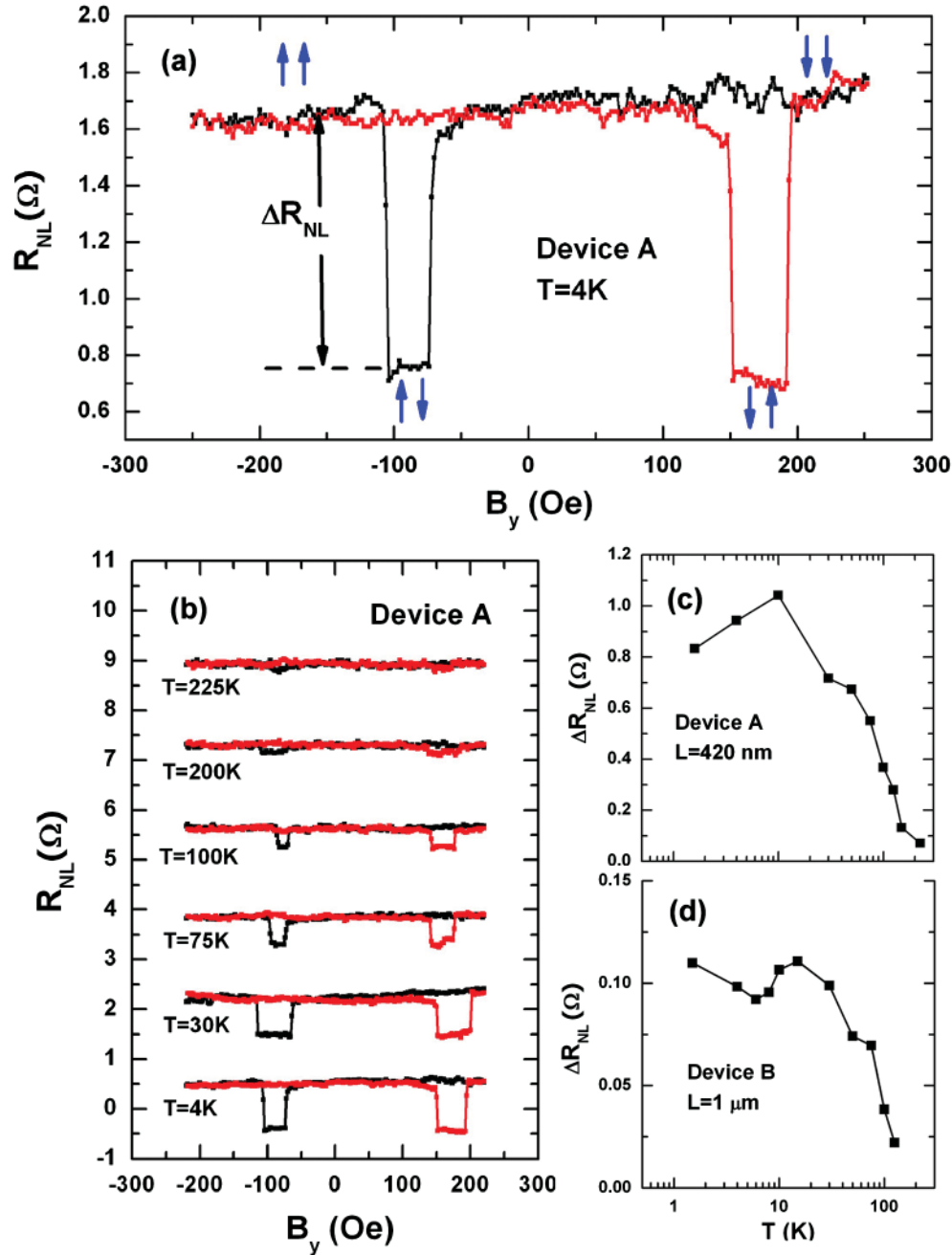


FIG. 2. (Color online) (a) Nonlocal spin valve signal measured on device A at 4 K with a DC injection current of -20 μA and AC injection current of -10 μA . The blue arrows indicate the magnetization directions of the injector and detector. (b) Temperature-dependent nonlocal spin valve signals on device A. The curves are offset for clarity. (c) and (d) Temperature-dependent nonlocal MR (ΔR_{NL}) of devices A and B, respectively.

directions of the spin injector (E2) and detector (E3) switch from parallel to antiparallel. To modulate the magnetization directions of the spin injector (E2) and detector (E3), an external magnetic field (B_y) along the easy axis of the electrodes [y direction as indicated in Fig. 1(b)] is swept, and the V_{NL} is recorded as a function of B_y . Figure 2(a) shows the nonlocal spin valve signal measured on device A at 4 K, with a reverse DC bias current (I_{DC}) of -20 μA and AC current (I_{AC}) of 10 μA . The nonlocal resistance R_{NL} is defined as the V_{NL} divided by I_{AC} . The difference of R_{NL} between the parallel

and antiparallel configuration is defined as the nonlocal MR (ΔR_{NL}) and measured to be 0.94 Ω in this case. Since we use the lock-in technique, the measured R_{NL} is characteristic of the slope of V_{NL} versus I_{DC} curve from the DC measurement. Therefore with the measured ΔR_{NL} of 0.94 Ω at -20 μA DC current bias, a DC nonlocal voltage of 18.8 μV can be obtained with a DC voltage bias of ~ 0.2 V. The Fermi levels of the Ge of different doping levels at 4 K are calculated to be 0.1 meV below the conduction band for the doping of $1 \times 10^{16} \text{cm}^{-3}$ and 1.4 meV, 9.1 meV, and 156.5 meV above the conduction

band for the doping of $1 \times 10^{17} \text{cm}^{-3}$, $1 \times 10^{18} \text{cm}^{-3}$, and $2 \times 10^{19} \text{cm}^{-3}$, respectively. Therefore the spin detection at 4 K is likely a measure of the spin accumulation in the graded doping layer. The spin injection efficiency of the Fe/MgO/Ge tunnel junction is estimated to be 0.23% using Eq. (1) in Ref. 19 with a spin diffusion length $\lambda_{sf} = 0.58 \mu\text{m}$ (calculated from nonlocal Hanle measurement), Ge conductivity $\sigma = 1 \text{S} \cdot \text{m}^{-1}$ (estimated from Ref. 29), cross-sectional area $A = 1.5 \mu\text{m}^2$, and $L = 420 \text{nm}$. The possible methods for improving the spin injection efficiency include the optimization the MgO film thickness and the Ge surface passivation technique.

Figure 2(b) shows the nonlocal spin valve signals measured on device A at different temperatures. The signal is observable up to 225 K. Figure 2(c) summarizes the ΔR_{NL} as a function of the temperature for device A. The ΔR_{NL} is weakly dependent on temperature at low temperature region, which increases slightly from 0.83Ω at 1.5 K to 1.04Ω at 10 K, and then decreases to 0.72Ω at 30 K. However, as the temperature further increases, the ΔR_{NL} drops abruptly and is not observable for $T > 225 \text{K}$. Similar temperature dependence of ΔR_{NL} is also observed in device B with a longer transport channel [$L = 1 \mu\text{m}$, as shown in Fig. 2(d)].

C. Non-local Hanle measurement

To further explore the spin transport properties in Ge, we perform the nonlocal Hanle measurement. In this measurement a small transverse [in z direction, as shown in Fig. 1(b)] magnetic field (B_z) is applied to induce the precession of the injected spin by the Hanle effect.^{21,30} The precession and dephasing of the spins during their transport in Ge is manifested as the magnetic field (B_z) dependence of the V_{NL} (or R_{NL} , equivalently). Figure 3(a) shows the Hanle precession curves of device B at 4 K under a reverse bias of $-130 \mu\text{A}$. The red and black symbols are for signals taken when the injector/detector magnetizations are in parallel and antiparallel configurations, respectively. A spin lifetime (τ_s) of 1.08 ns is extracted by fitting the Hanle curves based on the one-dimensional (1-D) spin drift diffusion model,^{18,19,22} under which

$$R_{\text{NL}} \propto \pm \int_0^\infty \frac{1}{\sqrt{4\pi Dt}} \exp\left[-\frac{L^2}{4Dt}\right] \cos(\omega_L t) \times \exp\left(-\frac{t}{\tau_s}\right) dt. \quad (1)$$

In the previous equation, + (−) sign is for the parallel (antiparallel) magnetization configuration, D is the diffusion constant, $\omega_L = g\mu_B B_z/\hbar$ is the Larmor frequency (where $g = 1.6$ is the Landé g -factor for Ge,³¹ μ_B is the Bohr magneton, and \hbar is the reduced Planck constant). The temperature-dependent spin lifetimes for device A and device B (obtained under reverse biases) are shown in Fig. 3(b) in solid circles and open squares, respectively. Similar to the temperature dependence of ΔR_{NL} , the dependence of the spin lifetime on temperature is rather weak at low temperatures, while it becomes much stronger as the temperature increases. This can be explained in the following. For Ge, which possesses the lattice-inversion symmetry, the spin relaxation is predicted to

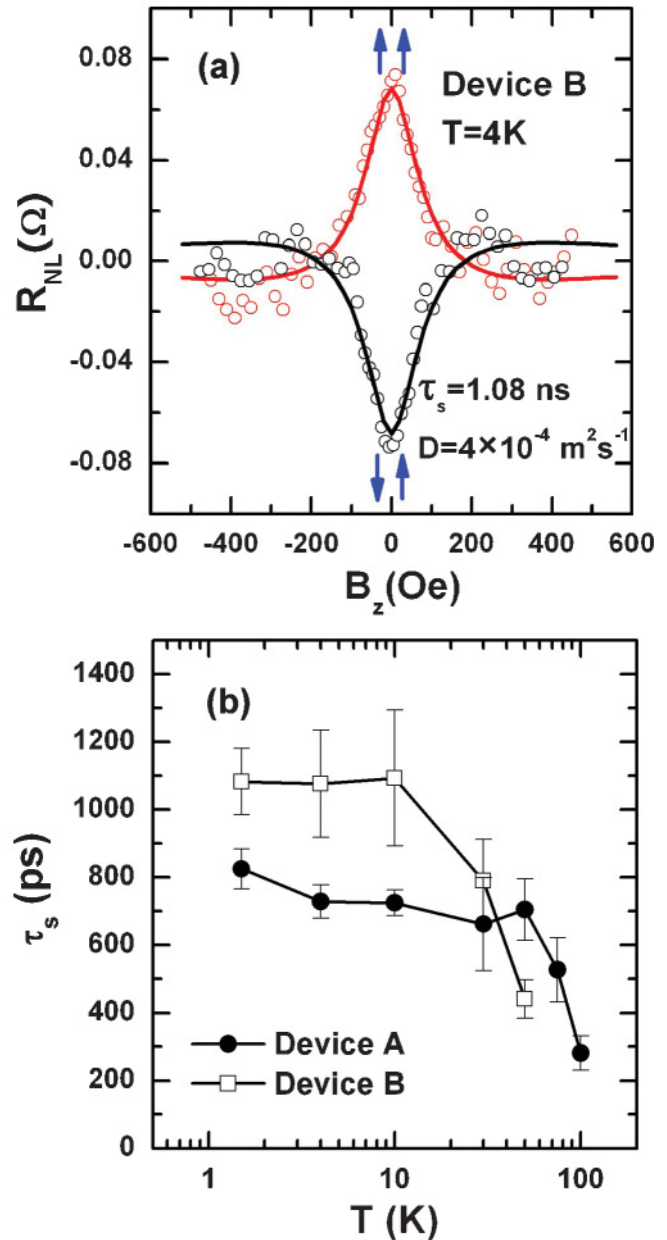


FIG. 3. (Color online) (a) Nonlocal Hanle precession curves measured on device B at 4 K with a DC injection current of $-130 \mu\text{A}$. The red and black symbols are for signals measured when the injector and detector are in parallel and antiparallel configurations, respectively. The solid lines are fitting based on the 1-D spin-drift diffusion model, from which the spin lifetime is extracted to be 1.08 ns. (b) Temperature-dependent spin lifetimes measured on device A (solid circles) and B (open squares), respectively.

be dominated by the Elliot-Yafet mechanism,^{12,13} under which the spin relaxation rate ($1/\tau_s$) is proportional to the momentum relaxation rate. The two major sources of momentum relaxation are the ionized impurity scattering and the phonon scattering. And the temperature dependence of the ionized impurity scattering rate is found to be much weaker than that of the phonon scattering in n-type Ge.²⁹ It is expected that at low temperature region, ionized impurity is the dominant

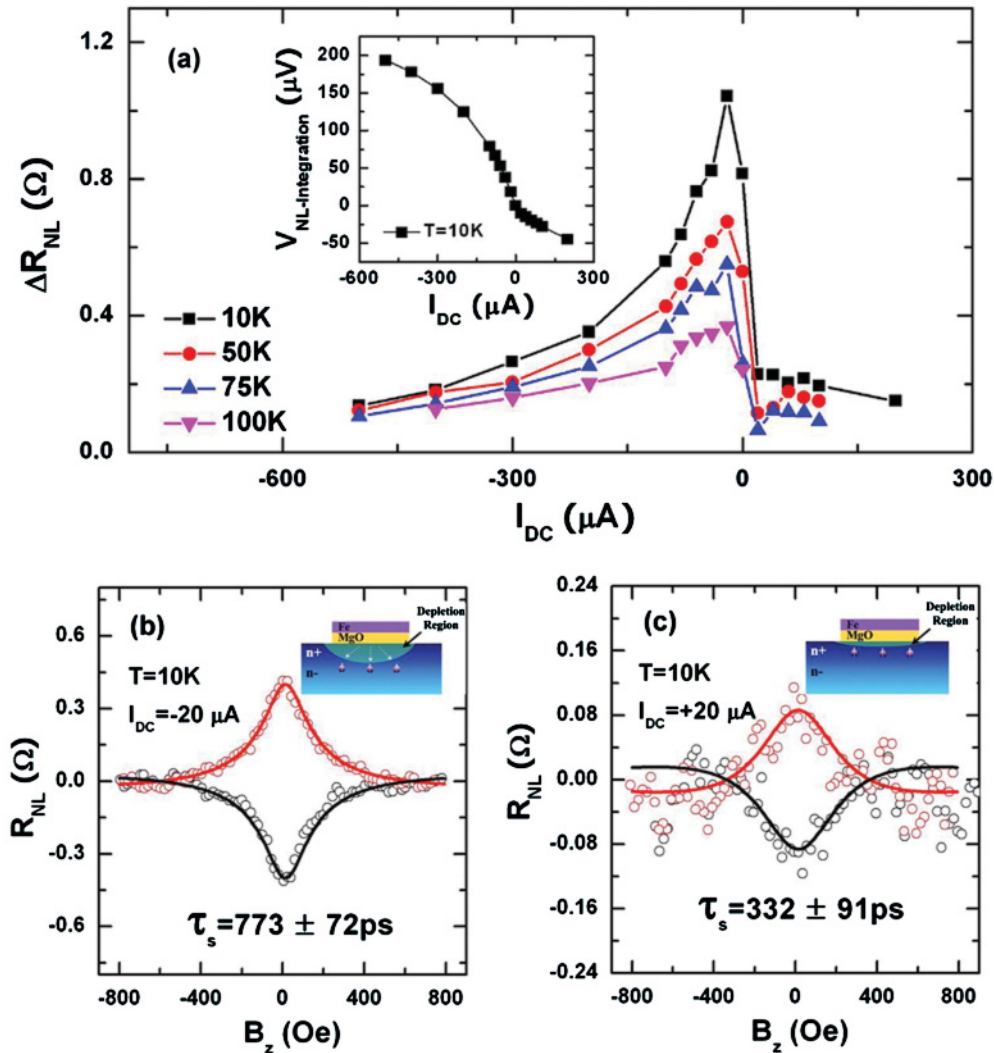


FIG. 4. (Color online) (a) The DC bias-dependent ΔR_{NL} of device A at different temperatures. The inset shows the restored DC relation between the V_{NL} and I_{DC} at 10 K by numerically integrating our V_{NL} over I_{DC} . (b) and (c) Hanle precession curves measured on device A at 10 K under a reverse bias of $-20 \mu\text{A}$ and a forward bias of $+20 \mu\text{A}$, respectively. The spin lifetimes extracted from the fittings (solid lines) based on the 1-D spin drift diffusion model are 773 ps and 332 ps for reverse and forward biases, respectively. The insets show the locations of the spin accumulation.

scattering source, therefore a weak temperature dependence of the spin relaxation rate (or spin lifetime, equivalently) is observed. As the temperature increases, phonon scattering becomes dominant, resulting in a much higher temperature dependence of the spin lifetime. Our results are consistent with the predicted Elliot-Yafet spin relaxation mechanism for Ge.

D. Bias dependence of the spin signals

Finally we study the bias dependence of the ΔR_{NL} and the spin lifetime. Figure 4(a) shows the DC bias-dependent ΔR_{NL} of device A at different temperatures. The inset of Fig. 4(a) shows the restored DC relation between the V_{NL} and I_{DC} at 10 K by numerically integrating our V_{NL} over I_{DC} . The bias dependence of V_{NL} at reverse bias is consistent with the

reported results on the Fe/GaAs system.¹⁸ However, our data do not display the nonmonotonic behavior at forward biases, which was attributed to the localized electrons in the surface bands due to the doping profile in the Fe/GaAs system.³² It is noted that the ΔR_{NL} is much smaller at forward biases as compared to those at reverse biases. Figure 4(b) and (c) shows the Hanle precession curves at 10 K with a DC reverse bias of $-20 \mu\text{A}$ and a forward bias of $+20 \mu\text{A}$, respectively. It is also found that the spin lifetime extracted from forward bias (332 ps) is shorter than that from the reverse bias (773 ps). The bias dependence of the ΔR_{NL} and spin lifetime can be explained by the doping-dependent spin relaxation, as found in the following. When a reverse bias is applied, the depletion region in the Ge extends and spin polarized electrons are injected into the lightly doped Ge channel [inset of Fig. 4(b)]. However, when a forward bias is applied, the depletion region is reduced, and the spin accumulates mainly at the highly doped

surface layer [inset of Fig. 4(c)], where a faster spin relaxation rate is expected due to the larger momentum scattering by ionized impurities. In addition to the doping-dependent spin relaxation, the bias dependence of the ΔR_{NL} could also be due to the following possible effects. First it could be due to the spin drift effect that arises from the unscreened electric field in the semiconductors. Since there is no charge current between injector and detector, the spin diffusion length does not change with bias in the direction toward the detector. However, in the other direction, the spin diffusion length will be highly dependent on the bias current, in which it will be longer when the electric field is along the diffusion direction (downstream), while it will be shorter when the electric field is opposite to the diffusion direction (upstream). The change of the spin diffusion length will have a significant effect on the spin injection efficiency, as explained by Yu and Flatte,^{33,34} when the electric field is higher than the critical field ($E_c \sim 15$ V/cm) in our case. Second it could also be due to interfacial tunneling asymmetry of the electrons tunneling out of and into the semiconductors from FM electrodes, in which the spin polarization is lower because of the reduced spin polarization at the hot electron states.³⁵ Third the spin-dependent interfacial electronic structure may also lead to a bias dependent ΔR_{NL} .³⁶ Further theoretical and experimental studies are needed to

elucidate the origin of the observed bias dependence of the spin signal.

IV. CONCLUSION

In conclusion we have successfully achieved electrical spin injection, transport, and detection in bulk n-type Ge by using an Fe/MgO/n-Ge tunnel junction. Investigating the temperature and bias dependence of the nonlocal spin valve signals and the spin lifetimes, we show that the spin relaxation in Ge is consistent with the predicted Elliot-Yafet mechanism. Our results present a major step towards achieving Ge and SiGe-based Spintronics devices for a new paradigm of nonvolatile electronics beyond CMOS technology.

ACKNOWLEDGMENTS

We gratefully acknowledge the financial support from the Western Institution of Nanoelectronics (WIN) through NRI. WH and RKK acknowledge support from NSF (CAREER DMR-0450037). The technical support from Jens Werner (IHT) and Olaf Kirfel (IHT) is also acknowledged. We thank Dmitri Nikonov, Ajey Jacob, and Charles Kuo of Intel Corporation and An Chen of Globalfoundries Corporation for the valuable discussion.

*These authors contributed equally to this work.

†Corresponding author: wang@ee.ucla.edu

¹S. A. Wolf, D. D. Awschalom, R. A. Buhrman, J. M. Daughton, S. von Molnar, M. L. Roukes, A. Y. Chtchelkanova, and D. M. Treger, *Science* **294**, 1488 (2001).

²I. Zutic, J. Fabian, and S. D. Sarma, *Rev. Mod. Phys.* **76**, 323 (2004).

³S. Datta and B. Das, *Appl. Phys. Lett.* **56**, 665 (1990).

⁴S. Sugahara and M. Tanaka, *Appl. Phys. Lett.* **84**, 2307 (2004).

⁵K. C. Hall and M. E. Flatte, *Appl. Phys. Lett.* **88**, 162503 (2006).

⁶International Technology Roadmap for Semiconductors, 2009 Edition [<http://www.itrs.net/reports.html>]. See Emerging Research Devices.

⁷I. Applebaum, B. Huang, and D. J. Monsma, *Nature*. **447**, 295 (2007).

⁸B. T. Jonker, G. Kioseoglou, A. T. Hanbicki, C. H. Li, and P. E. Thompson, *Nature Phys.* **3**, 542 (2007).

⁹S. P. Dash, S. Sharma, R. S. Patel, M. P. de Jong, and R. Jansen, *Nature*. **462**, 491 (2009).

¹⁰T. Suzuki, T. Sasaki, T. Oikawa, M. Shiraishi, Y. Suzuki, and K. Noguchi, *Appl. Phys. Express* **4**, 023003 (2011).

¹¹J.-M. Tang, B. T. Collins, and M. E. Flatte, e-print [arXiv:1104.0975v1](https://arxiv.org/abs/1104.0975v1) (2011).

¹²R. J. Elliott, *Phys. Rev.* **96**, 266 (1954).

¹³Y. Yafet, in *Solid State Physics*, edited by F. Seitz and D. Turnbull (Academic, New York, 1963), Vol. 14, p. 1.

¹⁴M. Oehme, J. Werner, and E. Kasper, *J. Cryst. Growth*. **310**, 4531 (2008).

¹⁵W. Han, Y. Zhou, Y. Wang, Y. Li, J. J. I. Wong, K. Pi, A. G. Swartz, K. M. McCreary, F. Xiu, K. L. Wang, J. Zou, and R. K. Kawakami, *J. Cryst. Growth* **312**, 44 (2009).

¹⁶Y. Zhou, W. Han, Y. Wang, F. Xiu, J. Zou, R. K. Kawakami, and K. L. Wang, *Appl. Phys. Lett.* **96**, 102103 (2010).

¹⁷W. H. Butler, X. G. Zhang, T. C. Schulthess, and J. M. MacLaren, *Phys. Rev. B* **63**, 054416 (2001).

¹⁸X. Lou, C. Adelman, S. A. Crooker, E. S. Garlid, J. Zhang, K. S. Madhukar Reddy, S. D. Flexner, C. J. Palmström, and P. A. Crowell, *Nature Phys.* **3**, 197 (2007).

¹⁹F. J. Jedema, H. B. Heersche, A. T. Filip, J. J. A. Baselmans, and B. J. van Wees, *Nature* **416**, 713 (2002).

²⁰O. van't Erve, C. Awo-Affouda, A. T. Hanbicki, C. H. Li, P. E. Thompson, and B. T. Jonker, *IEEE. Trans. Electron. Device* **56**, 2343 (2009).

²¹N. Tombros, C. Jozsa, M. Popinciuc, H. T. Jonkman, and B. J. van Wees, *Nature* **448**, 571 (2007).

²²W. Han, K. Pi, K. M. McCreary, Y. Li, J. J. I. Wong, A. G. Swartz, and R. K. Kawakami, *Phys. Rev. Lett.* **105**, 167202 (2010).

²³B. J. Jönsson-Åkerman, R. Escudero, C. Leighton, S. Kim, I. K. Schuller, and D. A. Rabson, *Appl. Phys. Lett.* **77**, 1870 (2000).

²⁴G. Schmidt, D. Ferrand, L. W. Molenkamp, A. T. Filip, and B. J. van Wees, *Phys. Rev. B* **62**, R4790 (2000).

²⁵E. I. Rashba, *Phys. Rev. B* **62**, R16267 (2000).

²⁶A. Fert and H. Jaffres, *Phys. Rev. B* **64**, 184420 (2001).

²⁷C. Ciuti, J. P. McGuire, and L. J. Sham, *Phys. Rev. Lett.* **89**, 156601 (2002).

²⁸J. Stephens, J. Berezovsky, J. P. McGuire, L. J. Sham, A. C. Gossard, and D. D. Awschalom, *Phys. Rev. Lett.* **93**, 097602 (2004).

²⁹P. P. Debye and E. M. Conwell, *Phys. Rev.* **93**, 693 (1954).

³⁰M. Johnson and R. H. Silsbee, *Phys. Rev. Lett.* **55**, 1790 (1985).

³¹G. Feher, D. K. Wilson, and E. A. Gere, *Phys. Rev. Lett.* **3**, 25 (1959).

³²H. Dery and L. J. Sham, *Phys. Rev. Lett.* **98**, 046602 (2007).

³³Z. G. Yu and M. E. Flatte, *Phys. Rev. B* **66**, 201202(R) (2002).

³⁴Z. G. Yu and M. E. Flatte, *Phys. Rev. B* **66**, 235302 (2002).

³⁵S. O. Valenzuela, D. J. Monsma, C. M. Marcus, V. Narayanamurti, and M. Tinkham, *Phys. Rev. Lett.* **94**, 196601 (2005).

³⁶A. N. Chantis, K. D. Belashchenko, D. L. Smith, E. Y. Tsybal, M. vanSchilfgaarde, and R. C. Albers, *Phys. Rev. Lett.* **99**, 196603 (2007).